Journal of Power Sources 245 (2014) 698–705

Contents lists available at SciVerse ScienceDirect

Journal of Power Sources

journal homepage: www.elsevier.com/locate/jpowsour

Enhanced electrochemical properties of Al_2O_3-coated LiV_3O_8 cathode materials for high-power lithium-ion batteries

S. Huang, J.P. Tu*, X.M. Jian, Y. Lu, S.J. Shi, X.Y. Zhao, T.Q. Wang, X.L. Wang, C.D. Gu

State Key Laboratory of Silicon Materials, Key Laboratory of Advanced Materials and Applications for Batteries of Zhejiang Province and Department of Materials Science and Engineering, Zhejiang University, Hangzhou 310027, China

HIGHLIGHTS

- Al_2O_3 was coated on the surface of LiV_3O_8 materials via a facile thermolysis process.
- A Li–V–Al–O solid solution forms at the LiV_3O_8/Al_2O_3 interface.
- The cyclic stability and high rate capability are improved due to Al_2O_3 coating.
- Al_2O_3 coating prevents particle bonding and deters irreversible phase transition.

ARTICLE INFO

Article history:
Received 2 May 2013
Received in revised form
5 July 2013
Accepted 6 July 2013
Available online 13 July 2013

Keywords:
Lithium trivanadate oxide
Surface modification
Aluminum oxide coating
Lithium-ion battery

ABSTRACT

Surface modified-LiV_3O_8 cathode materials with Al_2O_3 are successfully synthesized via a facile thermolysis process. The 0.5 wt.% Al_2O_3-coated LiV_3O_8 exhibits an enhanced cyclic stability at various charge–discharge current densities. At a current density of 100 mA g^{-1}, it delivers an initial specific discharge capacity of 283.1 mAh g^{-1} between 2.0 and 4.0 V. Moreover, high capacities of 139.4 and 118.5 mAh g^{-1} are obtained at the 100th cycle at current densities of 2000 and 3000 mA g^{-1}, respectively. The improved electrochemical performance is attributed to the Al_2O_3 coating, which can hinder the irreversible phase transformation and act as a protective layer to prevent the active material from direct contact with electrolyte. Furthermore, the formation of a Li–V–Al–O solid solution at the LiV_3O_8/Al_2O_3 interface provides a fast Li^+ diffusion path which is of benefit to the electrochemical behaviors.

1. Introduction

Rechargeable lithium ion batteries (LIBs) are widely used in portable electronic devices and hybrid electric vehicles because of their high energy density, long cycle life and environmental benign [1–3]. With the bottleneck of the development for LIBs nowadays, significant efforts should be made to reduce the cost and improve the electrochemical features which restrict the application of LIBs in electric vehicles and other fields [4–6].

Since 1950s, when it was firstly put forward, the layered lithium trivanadate (LiV_3O_8) cathode material has attracted extensive attention due to its low cost and high discharge capacity [7–9]. However, the LiV_3O_8 electrodes suffer from serious capacity loss and poor rate capability because there are incomplete reversible phase transformation and local structural damage during the insertion of lithium [10,11]. To date, many strategies have been utilized to improve the electrochemical performance of LiV_3O_8 such as doping [12–17] and structural/morphological modification [18–24]. For instance, Liu et al. [23] synthesized fluorine-doped lithium trivanadates $LiV_3O_{8-y}F_z$ by a solid-state reaction and found that the compound with $z = 0.1$ displayed good cyclic stability, high coulombic efficiency and good rate capability. In our previous work [24], freeze drying method was adopted to synthesize hierarchical plate-arrayed LiV_3O_8 compound which had good capacity retention and high-rate performance.

Besides, surface modification with phosphates [25–27], metal oxides [28–35] or other substances [36–41], have been demonstrated significant improvements in capacity retention of cathode materials. For instance, Jiao et al. [26] successfully

* Corresponding author. Tel.: +86 571 87952856; fax: +86 571 87952573.
E-mail addresses: tujp@zju.edu.cn, tujplab@zju.edu.cn (J.P. Tu).

0378-7753/$ – see front matter © 2013 Elsevier B.V. All rights reserved.
http://dx.doi.org/10.1016/j.jpowsour.2013.07.032

prepared $AlPO_4$-coated LiV_3O_8 powders by mixing active material LiV_3O_8 with $AlPO_4$ nanoparticle suspension followed by a low temperature heat treatment and the 1.0 wt.% $AlPO_4$-coated sample was found to reduce the capacity fade of LiV_3O_8 significantly. At 1.0 C, the 1.0 wt.% $AlPO_4$-coated LiV_3O_8 delivered an initial discharge capacity of 202.9 mAh g^{-1} between 1.8 and 4.0 V and the discharge capacity increased to 232 mAh g^{-1} at the 14th cycle with remaining 224 mAh g^{-1} after 60 cycles. While for metal oxide coatings, such as MgO, ZnO_2, ZrO_2, TiO_2 and so on, it has been reported that they do not take part in the electrochemical reactions [42,43]. Furthermore, they could act as protective layer to prevent the active core material from direct contact with electrolyte and suppress the dissolution of metal ions, thus improving the cyclic stability [44]. For example, Shi et al. [42] found that 2 wt.% MgO-coated $Li[Li_{0.2}Mn_{0.54}Ni_{0.13}Co_{0.13}]O_2$ could obtain a discharge capacity of 188.6 mAh g^{-1} after 100 cycles at 1 C with a high capacity retention of 96.4% of the initial cycle, while the bare one faded quickly from the initial discharge capacity of 236.6 mAh g^{-1} to 167.3 mAh g^{-1}. Similar to MgO coating, the surface modification of Al_2O_3 has been successfully applied to $LiCoO_2$ [45,46], $LiMn_2O_4$ [47], $LiCoPO_4$ [49] and $Li[Li_{0.05}Ni_{0.4}Co_{0.15}Mn_{0.4}]O_2$ [50]. However, to the best of our knowledge, Al_2O_3 coating has not yet been applied on the LiV_3O_8 cathode, whose capacity fades quickly during the charge and discharge processes.

In this present work, Al_2O_3 coating on the surface of LiV_3O_8 particles was carried out via a facile thermolysis of $Al(NO_3)_3$ process. The effect of the coating on the electrochemical performances, such as cyclic stability and high-rate capability, of the LiV_3O_8 cathodes were systematically investigated.

2. Experimental

All chemicals were used directly without further purification. Pristine LiV_3O_8 powder was synthesized by a classic peroxide sol–gel method [51]. To prepare Al_2O_3-coated LiV_3O_8 powders, certain amounts of $Al(NO_3)_3{\cdot}9H_2O$ (≥98%, Aladdin) were dissolved in distilled water firstly, then 1 g LiV_3O_8 powder was slowly poured into the $Al(NO_3)_3$ solution. The suspension containing the LiV_3O_8 powder was constantly stirred at 90 °C to evaporate water until it was dried. Finally, the dried mixtures were ground and then calcined at 500 °C for 90 min in air. The coated products with ratios of Al_2O_3/LiV_3O_8 = 0.2%, 0.5% and 1.5% in mass were synthesized, which were referred as AO02, AO05 and AO15 respectively for short. To explore the effect of Al_2O_3 coating, pristine LiV_3O_8 powder was also prepared at 500 °C by the same procedure, and the product was designated as AO0.

The morphologies and structures of the as-synthesized powders were characterized using field emission scanning electron microscopy (FESEM, FEI SIRION), Laser particle size instrument (LS-230 Coulter), high-resolution transmission electron microscopy (HRTEM, Tecnai G2 F20), X-ray diffraction (XRD, Rigaku D/max-2550 with graphite monochromated CuK_α radiation) and X-ray photo-electron spectroscopy (XPS, ESCALAB 250Xi). The binding energy scale of the XPS results was calibrated from the carbon contamination using the C 1s peak at 285.0 eV and core peaks were analyzed using a nonlinear Shirley-type background. The related peak positions and areas were optimized by a weighted least-squares fitting method.

Electrochemical performances of the as-synthesized LiV_3O_8 were investigated using CR2025 coin-type cell. The working electrodes were prepared by a slurry coating process. The slurry was composed of 80 wt.% active material, 15 wt.% carbon conductive agent (acetylene black, Ofluorine Chemical Co., Ltd., Shanghai) and 5 wt.% polyvinylidene fluoride (PVDF, SCM Industrial Chemical Co., Ltd., Shanghai) on aluminum foil. The cells were assembled in an argon-filled glove box (H_2O and O_2 concentrations below 1 ppm) with a metallic lithium foil as the anode, 1 M $LiPF_6$ in ethylene carbonate (EC)-dimethyl carbonate (DMC) (1:1 in volume) as the electrolyte (Zhangjiagang Guotai Huarong New Chemical Materials Co., Ltd), and a polypropylene micro-porous film (Cellgard 2300) as the separator. The galvanostatic discharge–charge tests were performed on a LAND battery program-control test system (Wuhan, China) between 2.0 and 4.0 V at current densities from 50 to 3000 mA g^{-1} at room temperature. Cyclic voltammetry (CV) tests were carried out on an electrochemical workstation (CHI604B) in the potential window of 2.0–4.0 V (vs. Li^+/Li) at a scan rate of 0.1 mV s^{-1}. Electrochemical impedance spectroscopy (EIS) measurements were performed on this apparatus using a three-electrode cell with the active material as the working electrode, metallic lithium foil as both the counter and reference electrodes. The amplitude of the AC signal was 5 mV over a frequency range from 100 kHz to 10 mHz at discharge states.

3. Results and discussion

3.1. Material characterization

Fig. 1 shows the XRD patterns of bare and various Al_2O_3-coated LiV_3O_8 powders. It can be seen that all the compounds are mainly made up of two phases, one is the main phase of the layered-type LiV_3O_8, which possesses a monoclinic crystalline structure and belongs to the P21/m space group (JCPDS 72-1193), the other is the impurity phase of $Li_{0.3}V_2O_5$ (JCPDS 73-1670), which can be commonly found in the LiV_3O_8 [21,22,24]. As an intercalation material, it has been found that the $Li_{0.3}V_2O_5$ could offer additional capacity to the total initial discharge capacity of the composite [22]. Recently, Bao et al. [52] has reported that $Li_{0.3}V_2O_5$ can be utilized as a promising material for aqueous LIBs, and when coupled with $LiCoO_2$, its first discharge capacity is 112 mAh g^{-1} at a current density of 180 mA g^{-1}. Accordingly, it can be assumed that the presence of $Li_{0.3}V_2O_5$ has a little influence on the total discharge capacity of the composites. In addition, the peaks arise at 2θ of 10.4 and 20.2° for AO0 can be attributed to another minor phase LiV_6O_{15} and V_2O_5, respectively. According to the pattern, the reflections are so small that little attention is paid to them. While for AO15, the small peak at 2θ of 11.0° is belonged to Al_2O_3, which is not observed in other samples because of the low amount. Besides, there is no apparent shift of peaks according to the standard patterns of

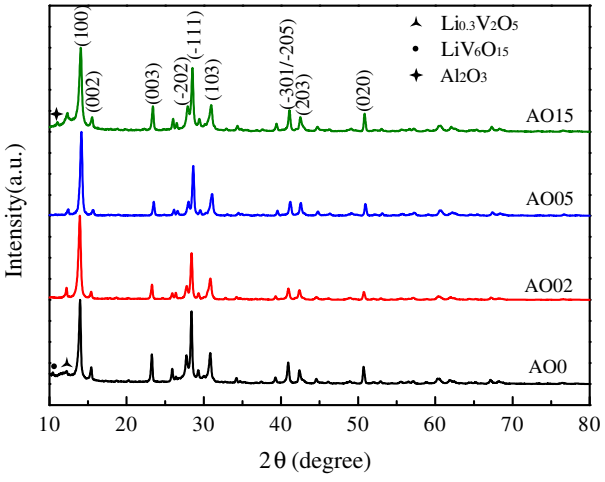

Fig. 1. XRD patterns of bare and various Al_2O_3-coated LiV_3O_8 powders.

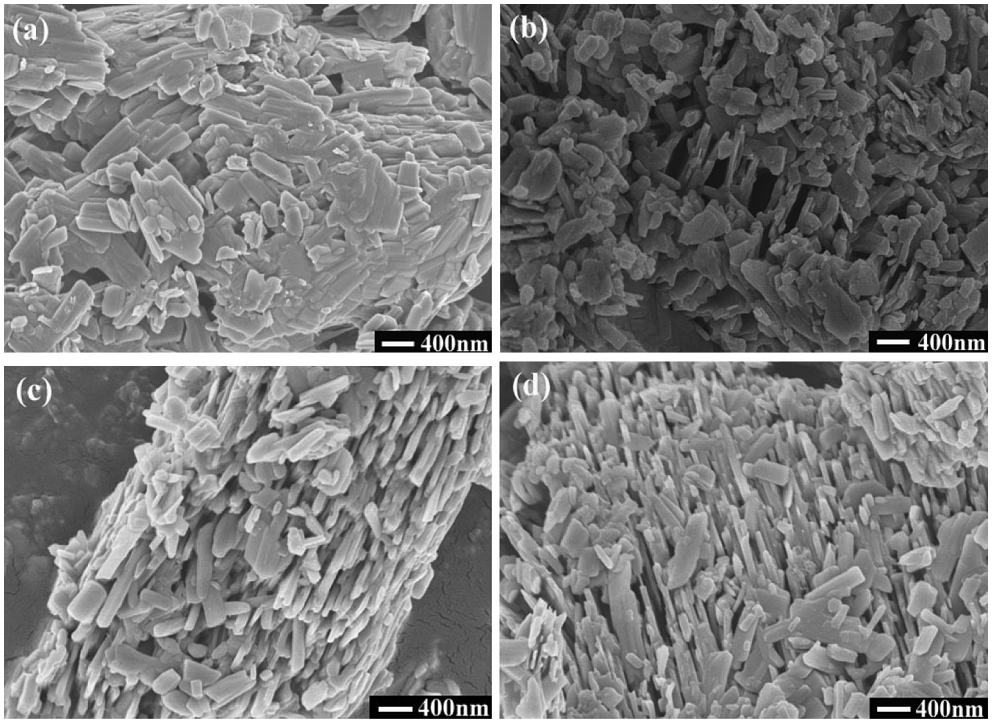

Fig. 2. SEM images of the pristine and Al_2O_3-coated LiV_3O_8 powders: (a) AO0, (b) AO02, (c) AO05 and (d) AO15.

LiV_3O_8, demonstrating that Al-doping in the body of the particles does not happen during the calcination process.

Fig. 2 shows the morphologies of the pristine and Al_2O_3-coated LiV_3O_8 powders. The thickness change of Al_2O_3 coating and mean particle diameter with different contents of Al_2O_3 coating are displayed in Table 1. It is obviously that AO0 exhibits an agglomeration of sheets (Fig. 2a) and the mean particle diameter is up to 2.681 μm. In the case of AO02, the particles seem to be smaller, whose sizes are 200–600 nm in length and 100–300 nm in width (Fig. 2b), and the result is approximately match with its mean particle diameter of 0.378 μm. However, for AO05 and AO15, most particles are well dispersed with clear profiles, still keeping the sheet-like morphology (Fig. 2c and d) with the mean particle diameter of 0.677 and 0.469 μm, respectively. Generally, the Al_2O_3-coated LiV_3O_8 particles seem to be much smaller and better shaped than the pristine ones. This may be ascribed to the coating process, which can prevent the particles from agglomeration. Such small and well-dispersed particles have advantages in the Li^+ insertion/extraction during cycling [11,53]. Fig. 3 shows the HRTEM images of the four powders. It is evident that the coating thickness increases with the content of Al_2O_3. To be more specific, the thickness of Al_2O_3 coating is 1.4–3 and 3–5 nm for AO02 and AO05 (Fig. 3b and c), respectively. However, when the content of Al_2O_3 coating increases to 1.5 wt.%, the coating thickness also increases to 6.8–11 nm (Fig. 3d). Besides, the lattice fringes and spacing in the body part of these particles are correspondingly in accordance with the indicated crystal plane of monoclinic LiV_3O_8.

Table 1
Thickness change of Al_2O_3 coating and mean particle diameter as different contents of Al_2O_3.

Sample	AO0	AO02	AO05	AO15
Al_2O_3 content/wt.%	0	0.2	0.5	1.5
Thickness of Al_2O_3 coating/nm	0	1.4–3	3–5	6.8–11
Mean particle diameter/μm	2.681	0.378	0.677	0.469

XPS measurements were carried out to analyze the surface composition and the oxidation state of the elements in Al_2O_3-coated LiV_3O_8 powder. The survey scan XPS spectrum of AO05 is shown in Fig. 4a. It is clear that the signals of Li, V and O appear on the spectrum. However, because the position of Al 2p is so close to V 3s that it cannot be distinctly revealed on the spectrum, special attention is paid on the high resolution XPS spectra which include the Al 2p core levels, as shown in Fig. 4b, it is corresponding to the red rectangle region indicated in Fig. 4a. By peak splitting and fitting, it is found that the binding energy of 69.8 eV belongs to V 3s. The Al 2p core level is composed of two peaks, the one at 74.3 eV corresponds to aluminum atoms in an oxygen environment, to be here, it is Al_2O_3, according to previous reports [54,55]. The other peak at 73.4 eV may be assigned to the formation of a solid solution of Li–V–Al–O at the interface between the coating and the core material, similar to the result of Verdier et al. [55]. On the other hand, to determine the oxidation degree of vanadium in vanadium oxide, the difference between the binding energy of O1s and $V2p_{3/2}$ should be taken into account. As shown in Fig. 4c, which corresponds to the blue rectangle region indicated in Fig. 4a, the peaks at 517.53 and 525.07 eV denote vanadium of +5 oxidation state in the composite. The O1s peak appears at 530.4 eV, and the difference of binding energy between $V2p_{3/2}$ and O1s is 12.87 eV. These results are in good match with what have been reported where the V^{5+} binding energy is 517.7 eV, and the difference of binding energy is 12.8 eV [56–58]. Based on the above experimental analysis, it can be concluded that the Al_2O_3 layer is uniformly coated on the

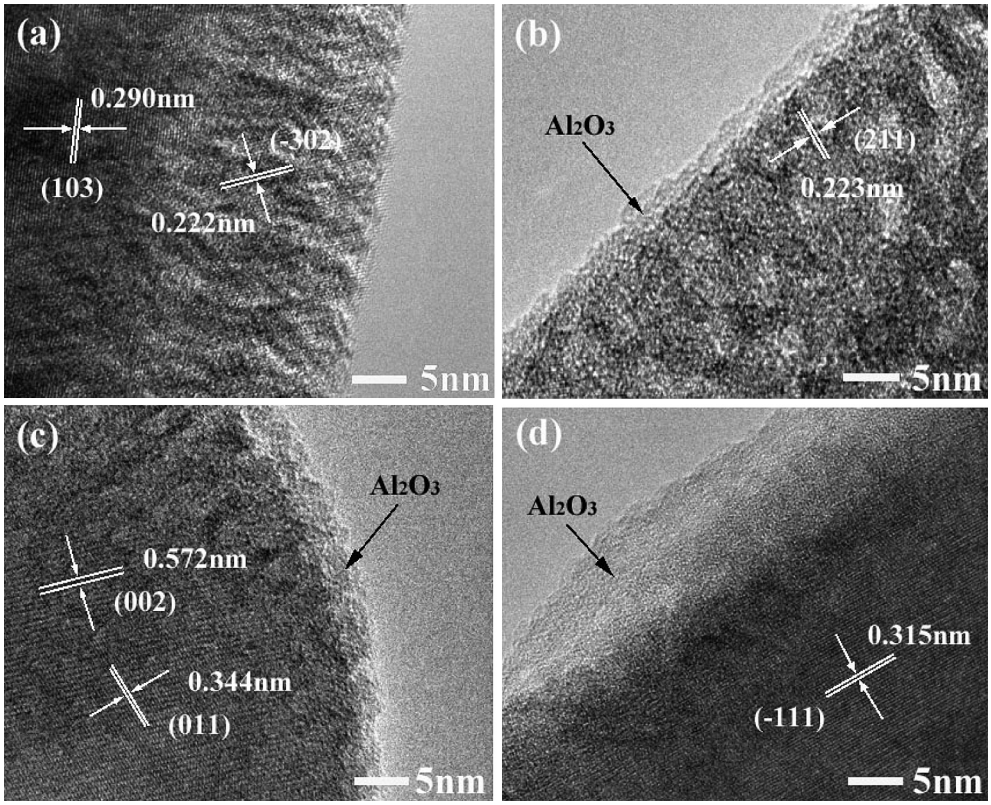

Fig. 3. HRTEM images of the pristine and Al_2O_3-coated LiV_3O_8 powders: (a) AO0, (b) AO02, (c) AO05 and (d) AO15.

surface of LiV_3O_8 particles and the deduced model of coating process is shown vividly in Fig. 5.

3.2. Electrochemical properties

To understand the effect of Al_2O_3 coating on the Li^+ intercalation/deintercalation behavior of LiV_3O_8, CV tests were performed at room temperature. Fig. 6 shows the initial four CV curves of the AO0 and AO05 electrodes in the potential range of 2.0–4.0 V (vs. Li^+/Li) at a scan rate of 0.1 mV s^{-1}. It is obvious that the first CV curves are a little different from the rest, due to the activation of the electrodes during the first scan [18,26]. Generally, there are about five main oxidation peaks (near 2.44, 2.48, 2.76, 2.85 and 3.67 V) and five main reduction peaks (near 2.29, 2.53, 2.72, 2.79 and 3.64 V) for both the electrodes, which can be assigned to several phase transformations between $Li_{1+x}V_3O_8$ ($x = 0.1–3$) couples [8,11,18,26]. The cathodic peaks around 2.63 and 2.87 V and the pair of anodic/cathodic peaks at 3.45 and 3.42 V are belonged to the impurity phase $Li_{0.3}V_2O_5$, as observed in the XRD patterns. According to Jouanneau et al. [11] and Kawakita et al. [8], the capacity fading of LiV_3O_8 materials mainly comes from two aspects: one is the two-phase transition phenomenon at ~2.6 V, which can be related to local damage of the crystal structure during the Li^+ insertion/extraction, thus leading to incomplete reversibility of phase transformation. The other aspect is the dissolution of small amount of V^{III} in the electrolyte. Comparing the two figures, it can be found that the current signal for the AO0 electrode gradually becomes small as cycling, especially for the oxidation peak at 2.76 V and the reduction peak at 2.53 V where a two-phase transformation occurs (Fig. 6a). However, this phenomenon does not exist for the AO05 electrode, indicating that the Al_2O_3 coating can hinder the irreversible phase transition of the LiV_3O_8 material, hence leading to enhanced cyclic stability (Fig. 6b). Furthermore, the cathodic/anodic peak positions of the Al_2O_3-coated LiV_3O_8 seem to have no change, indicating that the Al_2O_3 coating has little influence on the Li^+ intercalation/de-intercalation.

Fig. 7a shows the initial charge/discharge curves of the pristine LiV_3O_8 and Al_2O_3-coated LiV_3O_8 electrodes at a current density of 50 mA g^{-1} in the voltage range of 2.0–4.0 V. It is apparent that the curves of all the electrodes are of resemblance, displaying five main charge plateaus and five main discharge plateaus, which correspond to the CV results. Fig. 7b shows the cyclic performance of the pristine and Al_2O_3-coated LiV_3O_8 electrodes at a current density of 100 mA g^{-1} between 2.0 and 4.0 V at room temperature. Although the AO0 electrode delivers the highest initial specific discharge capacity of 309.1 mAh g^{-1}, it exhibits a poor cyclic capabilities, only 165.4 mAh g^{-1} can be obtained after 100 cycles. While for the Al_2O_3-coated LiV_3O_8, the initial specific discharge capacities seem to decrease, there are 263.6, 283.1 and 277.3 mAh g^{-1} for the AO02, AO05 and AO15 electrodes, respectively. A specific discharge capacity of 205.7 mAh g^{-1} can still be obtained after 100 cycles for AO05, much higher than that of AO02 (175.9 mAh g^{-1}) and AO15 (164 mAh g^{-1}). It seems that a proper coating of Al_2O_3 can improve the cyclic performance because the Al_2O_3 coating can prevent particles from agglomeration, meanwhile act as a shield to deter the irreversible phase transformation and protects the core material from direct contact with electrolyte [45,47]. Fig. 7c shows the rate capability of the LiV_3O_8 materials with or without Al_2O_3 coating between 2.0 and 4.0 V. Distinctly, the Al_2O_3-coated LiV_3O_8 electrodes have a better rate behavior than the pristine one. At a low current density of 30 mA g^{-1}, the AO05 electrode delivers a high specific discharge capacity of 302.6 mAh g^{-1}. With increasing the current density to 1500 mA g^{-1}, it still can deliver a capacity of 139.6 mAh g^{-1}, much higher than AO0 (85.9 mAh g^{-1}), AO02

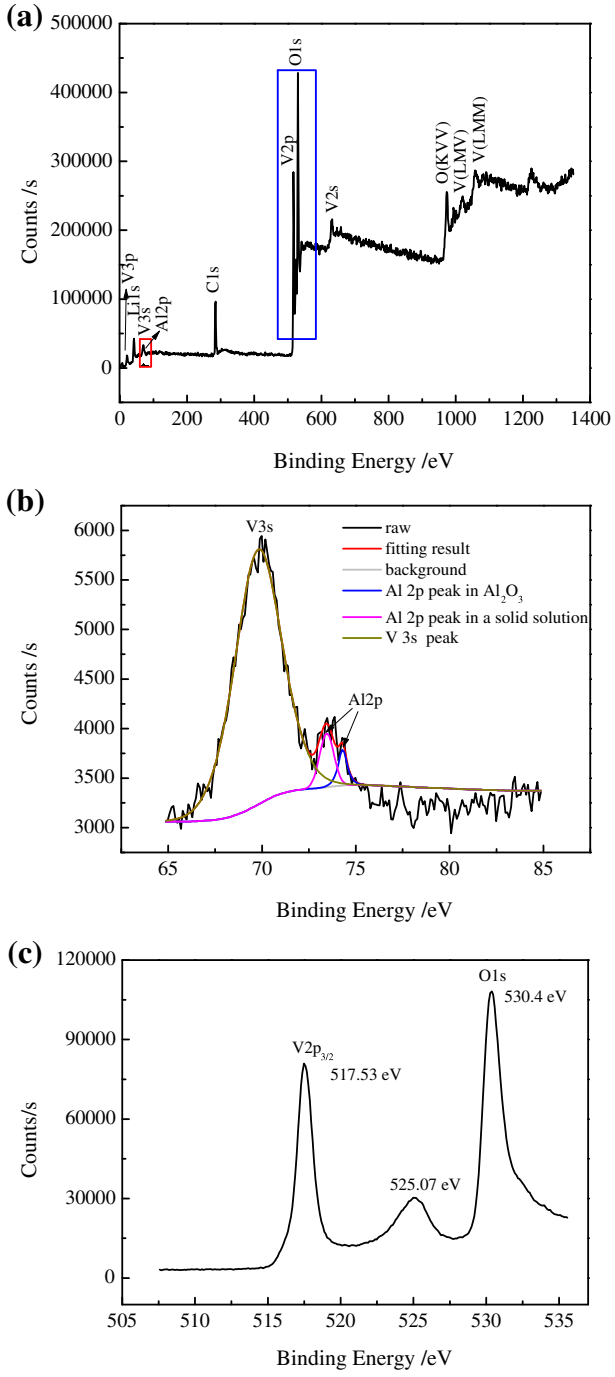

Fig. 4. XPS spectra of AO05 powder: (a) survey spectrum, (b) core-level spectra of V 3s and Al 2p, and (c) core-level spectra of V 2p and O 1s.

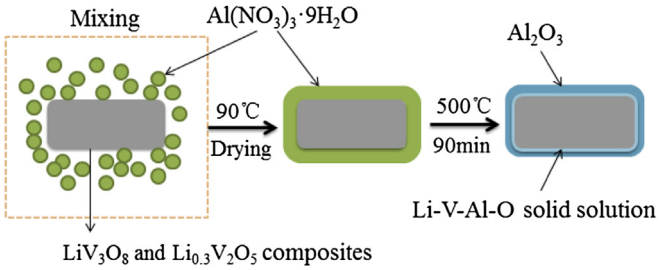

Fig. 5. Models of the coating process of Al_2O_3 on LiV_3O_8 particles.

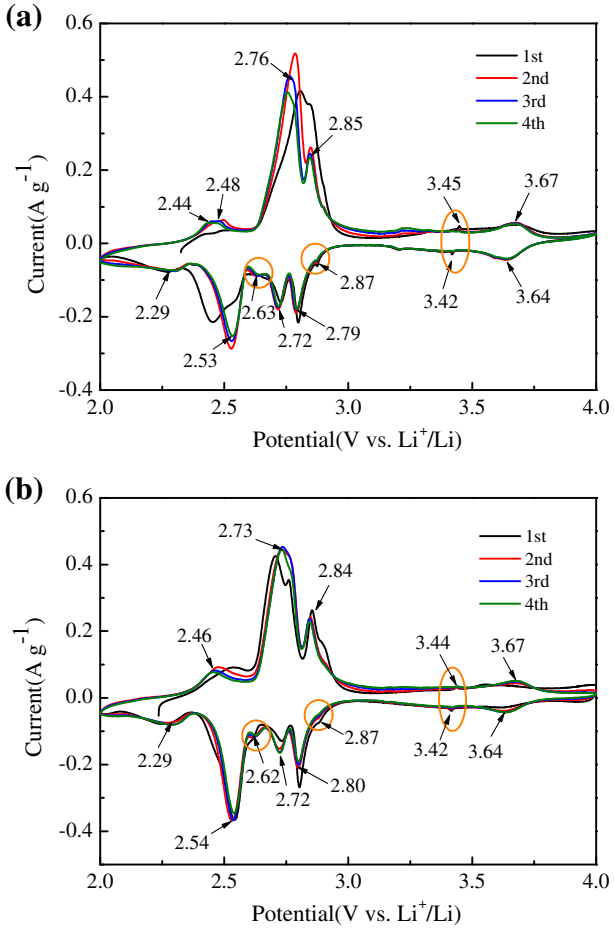

Fig. 6. CV curves of LiV_3O_8 electrodes at a scan rate of 0.1 mV s^{-1} in the potential range from 2.0 to 4.0 V (vs. Li^+/Li): (a) AO0 and (b) AO05.

(113.7 mAh g^{-1}) and AO15 (102.1 mAh g^{-1}). When the current density returns to 30 mA g^{-1}, the specific discharge capacity is only recovered to 234.3 mAh g^{-1} for AO0, while the AO05 electrode can recover to 260.9 mAh g^{-1}, revealing its good electrochemical reversibility.

The EIS test was carried out to further understand the electrochemical reaction kinetics of the Al_2O_3 coated LiV_3O_8. Fig. 8a and b shows the three-dimensional Nyquist plots for the AO0 and AO05 electrodes from the 3rd to the 100th cycle at a discharge state of 2.4 V, respectively. All the EIS spectra consist of a small intercept in the high frequency, two overlapped semicircles in the high to medium frequency and a quasi-straight line in the low frequency. Generally, the small intercept stands for the solution impedance of cell (R_e). The first semicircle in the high frequency is assigned to the impedance (R_{sl}) of Li^+ diffusion in the surface-passivating layer, another intermediate-frequency semicircle is related to the charge transfer impedance (R_{ct}) on the solid/electrolyte interface. And the quasi-straight line corresponds to the Warburg impedance of Li^+ diffusion in bulk material [22,48]. Fig. 8c shows the equivalent circuit used to fit the electrochemical impedance spectra, where C_{sl}, C_{dl}, and Z_W stand for the non-ideal capacitance of the surface-passivating layer, non-ideal capacitance of the double-layer the diffusion-controlled Warburg impedance, respectively. The simulated results of R_{sl} and R_{ct} of the two electrodes according to the equivalent circuit are presented in Fig. 9a and b, respectively. Table 2 shows the different impedance values and errors during the third and 100th cycles. It is clear that the R_{sl} and R_{ct} of the AO05

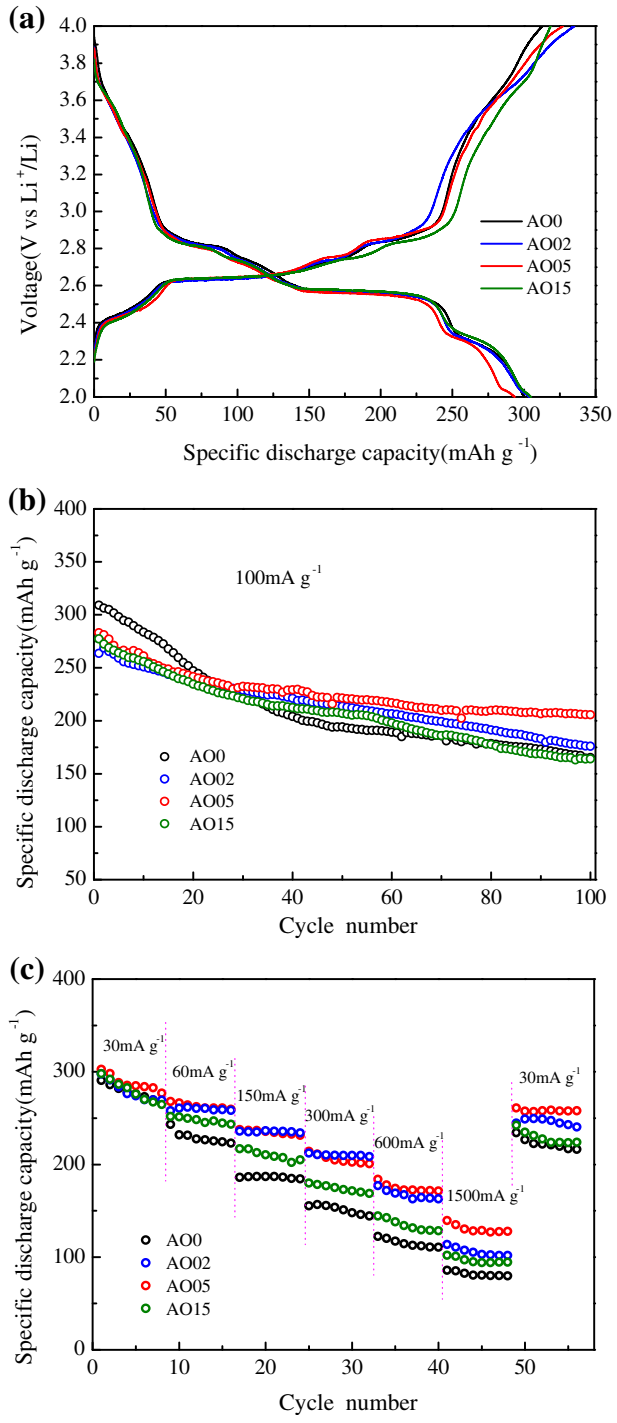

Fig. 7. (a) The initial charge/discharge curves of the pristine and Al_2O_3-coated LiV_3O_8 electrodes, (b) cyclic performance at a current density of 100 mA g^{-1}, (c) rate capacities of LiV_3O_8 electrodes at various current densities.

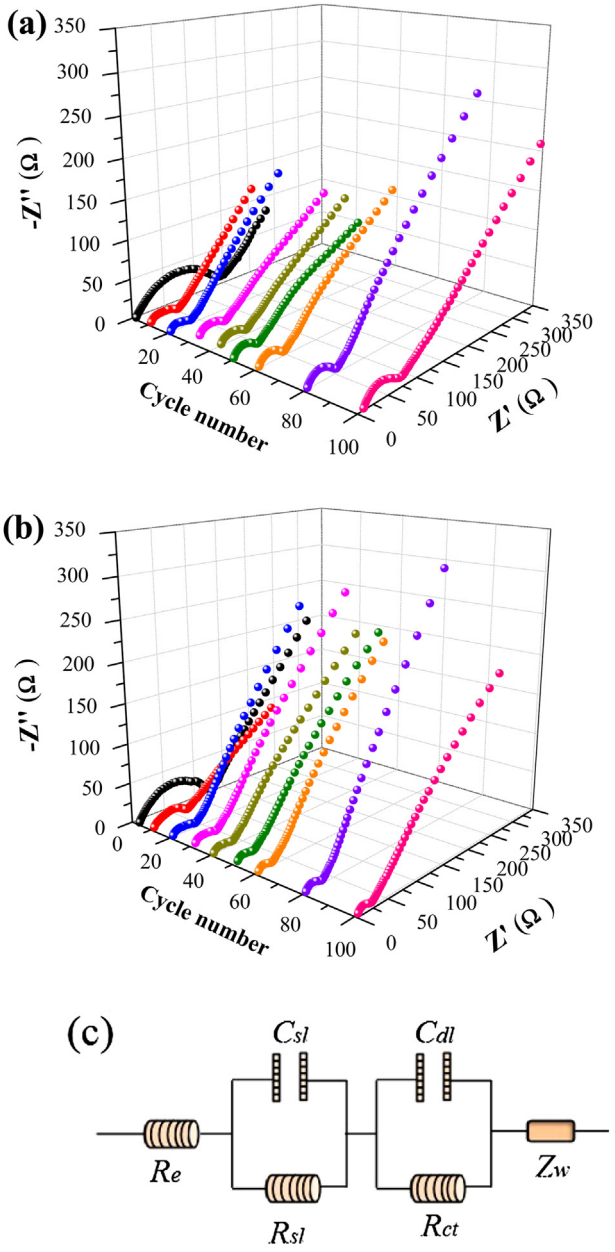

Fig. 8. Three-dimensional Nyquist plots for the LiV_3O_8 electrodes after cycling at the discharge state of 2.4 V: (a) AO0 (b) AO05, and (c) equivalent circuit model for the LiV_3O_8 electrodes.

electrode have a similar trend, both decreasing from the 3rd to the 20th cycle, then stabilizing around 15 Ω for R_{sl} and 7 Ω for R_{ct}, indicating the formation of a stable surface layer and fast electron transportation. While in case of the AO0 electrode, the R_{sl} and R_{ct} vary with ups and downs during cycling and mostly have higher values than those of AO05, indicating higher polarization of the electrode [6]. Furthermore, the fluctuations may be attributed to the absence of Al_2O_3 coating, which can restrict the thickening or deposition of SEI film during the charge/discharge processes [22,42]. Moreover, the well-dispersed particles, as shown in Fig. 2, can favor in faster Li^+ diffusion and electron transportation, thus leading to a low value of R_{ct} for the AO05 electrode.

To further promote the application of the LiV_3O_8 materials, the high-rate capability of the AO0 and AO05 electrodes was compared. As shown in Fig. 10, the AO05 electrode can deliver high initial specific discharge capacities of 195.5 and 160.2 mAh g^{-1} at current densities of 2000 and 3000 mA g^{-1}, respectively. Even after 100 cycles, it can retain 139.4 and 118.5 mAh g^{-1} for each other. As for the AO0 electrode, only 91.7 and 74.2 mAh g^{-1} are attained from the initial specific discharge capacities of 170.6 and 134.2 mAh g^{-1}, and the capacity retention is 53.8 and 55.3% at the 100th cycle, respectively. Besides the well-dispersed morphology, improved

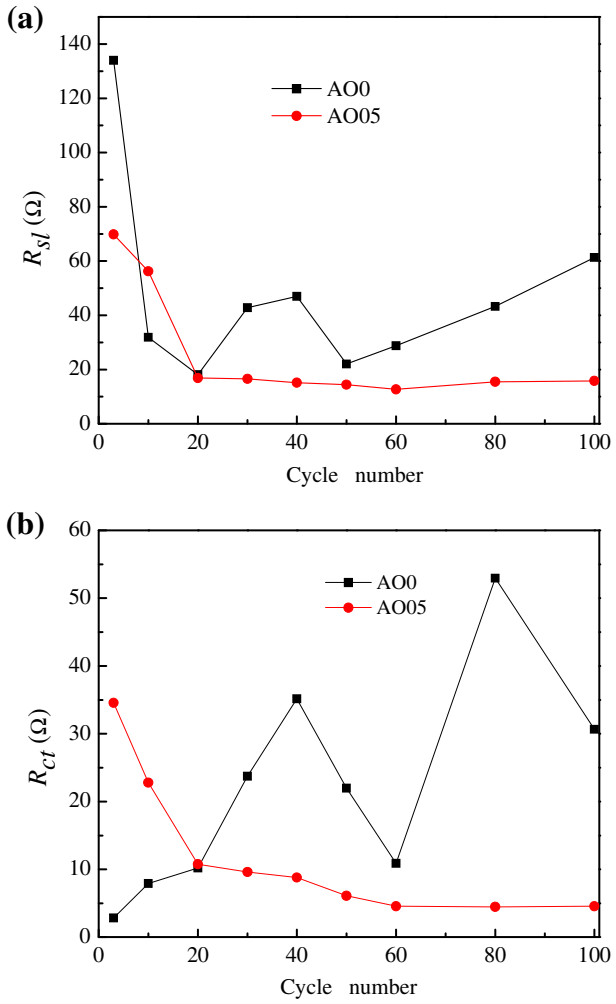

Fig. 9. Variation of (a) R_{sl} and (b) R_{ct} during cycling calculated from fitting the Nyquist plots.

structural stability and depressed interaction between the core material and electrolyte, the possible formation of the Li–V–Al–O solid solution at the LiV_3O_8/Al_2O_3 interface are of benefit to the electrochemical behaviors at high current densities. Enhanced Li^+ diffusion due to the formation of such a solid solution has also been reported for the formation of a $LiCo_{1-x}Al_xPO_z$ [49] or $LiCo_{1-x}Al_xO_z$ [59,60] solid solution. Hence, the 0.5 wt.% Al_2O_3-coated LiV_3O_8 electrode has a better high-rate cyclic performance than the pristine one.

Table 2
Impedance values during the third and 100th cycles.

Cycles	AO0				AO05			
	R_e	R_{sl}	R_{ct}	Chi-squared	R_e	R_{sl}	R_{ct}	Chi-squared
3rd	2.04	134	2.81	1.05E-03	2.75	69.82	34.55	2.00E-03
10th	4.75	31.89	7.91	5.98E-04	4.02	56.20	22.80	1.98E-03
20th	5.00	18.09	10.20	6.80E-04	2.84	16.89	10.75	1.33E-03
30th	16.81	42.75	23.75	2.45E-04	8.28	16.57	9.62	1.78E-03
40th	5.20	46.99	35.16	1.57E-03	4.46	15.15	8.80	9.45E-04
50th	3.07	22.04	21.96	8.92E-04	8.32	14.43	6.11	6.40E-04
60th	6.29	28.77	10.90	2.65E-04	5.89	12.69	4.55	2.11E-03
80th	4.96	43.25	52.95	4.66E-04	7.41	15.53	4.47	2.60E-03
100th	8.76	61.35	30.64	3.64E-04	4.83	15.78	4.56	1.27E-03

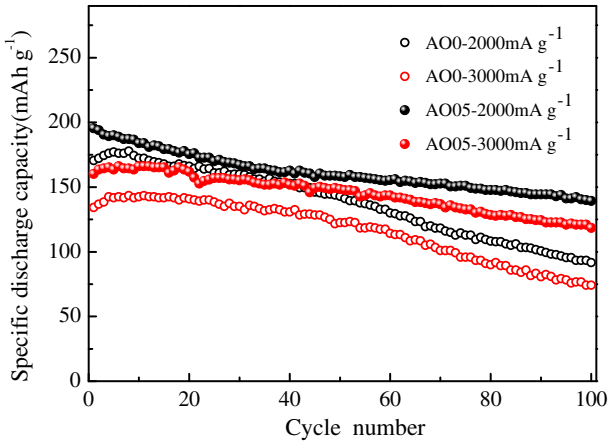

Fig. 10. Cyclic performances of the AO0 and AO05 electrodes at high charge–discharge current densities between 2.0 and 4.0 V.

4. Conclusions

Surface modified-LiV_3O_8 materials with Al_2O_3 were successfully synthesized via a facile thermolysis process. The 0.5 wt.% Al_2O_3-coated LiV_3O_8 has improved cyclic performances at different current densities than the pristine one since the coating can prevent particle agglomeration, deter the irreversible phase transformation and act as a protective layer to prevent the active material from direct contact with electrolyte. Besides, the formation of a Li–V–Al–O solid solution at the LiV_3O_8/Al_2O_3 interface provides a faster Li^+ diffusion path which can favor the electrochemical properties. Even at the current densities of 2000 and 3000 mA g^{-1}, high specific discharge capacities of 139.4 and 118.5 mAh g^{-1} can still be obtained after 100 cycles for the 0.5 wt.% Al_2O_3-coated LiV_3O_8 electrode. The LiV_3O_8 with proper Al_2O_3 coating has a promising application as the cathode material for high-power lithium ion batteries.

Acknowledgments

This work was supported by the Key Science and Technology Innovation Team of Zhejiang Province (2010R50013). The authors also thank the help of Mr. Wei Huang and Ms. Fu Liu for operating the TEM and XPS, respectively.

References

[1] Y. Wang, G.Z. Cao, Adv. Mater. 20 (2008) 2251.
[2] C. Liu, F. Li, L.-P. Ma, H.-M. Cheng, Adv. Mater. 22 (2010) E28.
[3] K. Saravanan, K. Ananthanarayanan, P. Balaya, Energy Environ. Sci. 3 (2010) 939.
[4] J.-M. Tarascon, M. Armand, Nature 414 (2001) 359.
[5] J.B. Goodenough, Y. Kim, Chem. Mater. 22 (2010) 587.
[6] Y.Q. Qiao, X.L. Wang, Y.J. Mai, J.Y. Xiang, D. Zhang, C.D. Gu, J.P. Tu, J. Power Sources 196 (2011) 8706.
[7] S. Panero, M. Pasquali, G. Pistoia, J. Electrochem. Soc. 130 (1983) 1225.
[8] J. Kawakita, T. Miura, T. Kishi, J. Power Sources 83 (1999) 79.
[9] X.-W. Gao, J.-Z. Wang, S.-L. Chou, H.-K. Liu, J. Power Sources 220 (2012) 47.
[10] R. Benedek, M.M. Thackeray, L.H. Yang, J. Power Sources 81 (1999) 487.
[11] S. Jouanneau, A. Le Gal La Salle, A. Verbaere, D. Guyomard, J. Electrochem. Soc. 152 (2005) A1660.
[12] L. Liu, L.F. Jiao, J.L. Sun, Y.H. Zhang, M. Zhao, H.T. Yuan, Y.M. Wang, Electrochim. Acta 53 (2008) 7321.
[13] S.V. Pouchko, A.K. Ivanov-Schitz, T.L. Kulova, A.M. Skundin, E.P. Turevskaya, Solid State Ionics 151 (2002) 129.
[14] Y. Feng, Y.L. Li, F. Hou, J. Power Sources 187 (2009) 224.
[15] C.Q. Feng, L.F. Huang, Z.P. Guo, J.Z. Wang, H.K. Liu, J. Power Sources 174 (2007) 548.
[16] M. Zhao, L.F. Jiao, H.T. Yuan, Y. Feng, M. Zhang, Solid State Ionics 178 (2007) 387.

[17] J.W. Fergus, J. Power Sources 195 (2010) 939.
[18] Y.Q. Qiao, X.L. Wang, J.P. Zhou, J. Zhang, C.D. Gu, J.P. Tu, J. Power Sources 198 (2012) 287.
[19] A.Q. Pan, J.-G. Zhang, G.Z. Cao, S.Q. Liang, C.M. Wang, Z.M. Nie, B.W. Arey, W. Xu, D.W. Liu, J. Xiao, G.S. Li, J. Liu, J. Mater. Chem. 21 (2011) 10077.
[20] H. Ma, Z.Q. Yuan, F.Y. Cheng, J. Liang, Z.L. Tao, J. Chen, J. Alloys Compd. 509 (2011) 6030.
[21] A.Q. Pan, J. Liu, J.-G. Zhang, G.Z. Cao, W. Xu, Z.M. Nie, X. Jie, D.W. Choi, B.W. Arey, C.M. Wang, S.Q. Liang, J. Mater. Chem. 21 (2011) 1153.
[22] Y.Q. Qiao, J.P. Tu, X.L. Wang, J. Zhang, Y.X. Yu, C.D. Gu, J. Phys. Chem. C 115 (2011) 25508.
[23] Y.M. Liu, X.C. Zhou, Y.L. Guo, Electrochim. Acta 54 (2009) 3184.
[24] S. Huang, Y. Lu, T.Q. Wang, C.D. Gu, X.L. Wang, J.P. Tu, J. Power Sources 235 (2013) 256.
[25] J. Kim, M. Noh, J. Cho, H. Kim, K. Kim, J. Electrochem. Soc. 152 (2005) A1142.
[26] L.F. Jiao, L. Liu, J.L. Sun, L. Yang, Y.H. Zhang, H.T. Yuan, Y.M. Wang, X.D. Zhou, J. Phys. Chem. C 112 (2008) 18249.
[27] L.-L. Xie, L.-Q. You, X.-Y. Cao, C.-F. Zhang, D.-W. Song, L.-B. Qu, Electron. Mater. Lett. 8 (2012) 411.
[28] H.L. Zhao, L. Gao, W.H. Qiu, X.H. Zhang, J. Power Sources 132 (2004) 195.
[29] L.H. Yu, X.P. Qiu, J.Y. Xi, W.T. Zhu, L.Q. Chen, Electrochim. Acta 51 (2006) 6406.
[30] D.C. Li, Y. Kato, K. Kobayakawa, H. Noguchi, Y. Sato, J. Power Sources 160 (2006) 1342.
[31] H.S. Liu, Z.R. Zhang, Z.L. Gong, Y. Yang, Solid State Ionics 166 (2004) 317.
[32] K.-S. Lee, S.-T. Myung, H. Bang, K. Amine, D.-W. Kim, Y.-K. Sun, J. Power Sources 189 (2009) 494.
[33] Y.J. Kim, J. Cho, T.-J. Kim, B. Park, J. Electrochem. Soc. 150 (2003) A1723.
[34] Z. Wang, X. Huang, L. Chen, J. Electrochem. Soc. 150 (2003) A199.
[35] J. Cho, C.-S. Kim, S.-I. Yoo, Electrochem. Solid-State Lett. 3 (2000) 362.
[36] F.H. Tian, L. Liu, Z.H. Yang, X.Y. Wang, Q.Q. Chen, X.Y. Wang, Mater. Chem. Phys. 127 (2011) 151.
[37] N.H. Idris, M.M. Rahman, J.-Z. Wang, Z.-X. Chen, H.-K. Liu, Compos. Sci. Technol. 71 (2011) 343.
[38] Y. Zhou, H.-F. Yue, X.-Y. Zhang, X.-Y. Deng, Solid State Ionics 179 (2008) 1763.
[39] X.-Y. Cao, L.-J. Guo, J.-P. Liu, L.-L. Xie, Int. J. Electrochem. Sci. 6 (2011) 270.
[40] K.-S. Lee, S.-T. Myung, D.-W. Kim, Y.-K. Sun, J. Power Sources 196 (2011) 6974.
[41] S.J. Shi, J.P. Tu, Y.Y. Tang, Y.Q. Zhang, X.Y. Liu, X.L. Wang, C.D. Gu, J. Power Sources 225 (2013) 338.
[42] S.J. Shi, J.P. Tu, Y.Y. Tang, X.Y. Liu, Y.Q. Zhang, X.L. Wang, C.D. Gu, Electrochim. Acta 88 (2013) 671.
[43] J.T. Lee, F.M. Wang, C.S. Cheng, C.C. Li, C.H. Lin, Electrochim. Acta 55 (2010) 4002.
[44] H. Liu, Y.P. Wu, E. Rahm, R. Holze, H.Q. Wu, J. Solid State Electrochem. 8 (2004) 450.
[45] L.J. Liu, Z.X. Wang, H. Li, L.Q. Chen, X.J. Huang, Solid State Ionics 152 (2002) 341.
[46] S. Oh, J.K. Lee, D. Byun, W.I. Cho, B.W. Cho, J. Power Sources 132 (2004) 249.
[47] W.-K. Kim, D.-W. Han, W.-H. Ryu, S.-J. Lim, H.-S. Kwon, Electrochim. Acta 71 (2012) 17.
[48] J.Y. Xiang, J.P. Tu, Y.Q. Qiao, X.L. Wang, J. Zhong, D. Zhang, C.D. Gu, J. Phys. Chem. C 115 (2011) 2505.
[49] A. Eftekhari, J. Electrochem. Soc. 151 (2004) A1456.
[50] S.-T. Myung, K. Izumi, S. Komaba, H. Yashiro, H.J. Bang, Y.-K. Sun, N. Kumagai, J. Phys. Chem. C 111 (2007) 4061.
[51] J.J. Feng, X.Z. Liu, X.M. Zhang, J.Z. Jiang, J. Zhao, M. Wang, J. Electrochem. Soc. 156 (2009) A768.
[52] J. Bao, M. Zhou, Y.Q. Zeng, L.F. Bai, X.D. Zhang, K. Xu, Y. Xie, J. Mater. Chem. A 1 (2013) 5423.
[53] S. Jouanneau, A. Le Gal La Salle, A. Verbaere, M. Deschamps, S. Lascaud, D. Guyomard, J. Mater. Chem. 13 (2003) 921.
[54] M.R. Alexander, G. Beamson, P. Bailey, T.C.Q. Noakes, P. Skeldon, G.E. Thompson, Surf. Interface Anal. 35 (2003) 649.
[55] S. Verdier, L. El Ouatani, R. Dedryvère, F. Bonhomme, P. Biensan, D. Gonbeau, J. Electrochem. Soc. 154 (2007) A1088.
[56] J. Mendialdua, R. Casanova, Y. Barbaux, J. Electron. Spectrosc. 71 (1995) 249.
[57] X.H. Liu, J.Q. Wang, J.Y. Zhang, S.R. Yang, J. Mater. Sci. 42 (2007) 867.
[58] G. Silversmit, D. Depla, H. Poelman, G.B. Marin, R.D. Gryse, J. Electron. Spectrosc. 135 (2004) 167.
[59] J.D. Perkins, C.S. Bahn, J.M. McGraw, P.A. Parilla, D.S. Ginley, J. Electrochem. Soc. 148 (2001) A1302.
[60] Y.J. Kim, T.-J. Kim, J.W. Shin, B. Park, J. Cho, J. Electrochem. Soc. 149 (2002) A1337.